Report Documentation Page

1. REPORT DATE **APR 2007**	2. REPORT TYPE	3. DATES COVERED **00-00-2007 to 00-00-2007**

4. TITLE AND SUBTITLE **The Effect Of Rotation On Calibrators For Ground-based Interferometry**	5a. CONTRACT NUMBER
	5b. GRANT NUMBER
	5c. PROGRAM ELEMENT NUMBER

6. AUTHOR(S)	5d. PROJECT NUMBER
	5e. TASK NUMBER
	5f. WORK UNIT NUMBER

7. PERFORMING ORGANIZATION NAME(S) AND ADDRESS(ES) **U.S. Naval Observatory,3450 Massachusetts Avenue, N.W.,Washington,DC,20392**	8. PERFORMING ORGANIZATION REPORT NUMBER

9. SPONSORING/MONITORING AGENCY NAME(S) AND ADDRESS(ES)	10. SPONSOR/MONITOR'S ACRONYM(S)
	11. SPONSOR/MONITOR'S REPORT NUMBER(S)

12. DISTRIBUTION/AVAILABILITY STATEMENT
Approved for public release; distribution unlimited

14. ABSTRACT
We consider the problem introduced by rotation in the use of early-type stars as calibrators for optical interferometry. These objects have high surface brightnesses and hence are relatively bright, even with small angular diameters. However, rotation can introduce changes in the predicted visibilities well in excess of the uncertainties in the various diameter-magnitude-color calibrations. Measurements of the projected rotational velocity constrain these effects, but the constraints are complicated and not easily evaluated when selecting potential calibrators. Furthermore, the magnitude of the variations depends on the details of the interferometer,such as latitude, baseline length, and operating wavelength. Nevertheless, using measured magnitudes, colors parallaxes, and projected rotational velocities, and estimating masses from standard evolutionary grids, we are able to calculate histograms that approximate the probability distribution of the visibilities and allow us to characterize the width of the distribution of squared visibilities and the total range induced by rotation. We have found that proximity to the ZAMS adds a valuable constraint, allowing stars with moderate rotation to be reliable calibrators in a number of cases. Catalogs characterizing the sensitivity of the visibilities of potential calibrators to rotation are presented for a number of standard interferometer configurations.

15. SUBJECT TERMS

16. SECURITY CLASSIFICATION OF:			17. LIMITATION OF ABSTRACT	18. NUMBER OF PAGES	19a. NAME OF RESPONSIBLE PERSON
a. REPORT **unclassified**	b. ABSTRACT **unclassified**	c. THIS PAGE **unclassified**	**Same as Report (SAR)**	**9**	

The Effect of Rotation on Calibrators for Ground-based Interferometry

Jinmi Yoon,[1] Deane M. Peterson,[1] J. Thomas Armstrong,[2] James H. Clark III,[2] G. Charmaine Gilbreath,[2]
Thomas Pauls,[2] Henrique R. Schmitt,[2,3] and Robert J. Zagarello[4]

ABSTRACT.   We consider the problem introduced by rotation in the use of early-type stars as calibrators for optical interferometry. These objects have high surface brightnesses and hence are relatively bright, even with small angular diameters. However, rotation can introduce changes in the predicted visibilities well in excess of the uncertainties in the various diameter-magnitude-color calibrations. Measurements of the projected rotational velocity constrain these effects, but the constraints are complicated and not easily evaluated when selecting potential calibrators. Furthermore, the magnitude of the variations depends on the details of the interferometer, such as latitude, baseline length, and operating wavelength. Nevertheless, using measured magnitudes, colors, parallaxes, and projected rotational velocities, and estimating masses from standard evolutionary grids, we are able to calculate histograms that approximate the probability distribution of the visibilities and allow us to characterize the width of the distribution of squared visibilities and the total range induced by rotation. We have found that proximity to the ZAMS adds a valuable constraint, allowing stars with moderate rotation to be reliable calibrators in a number of cases. Catalogs characterizing the sensitivity of the visibilities of potential calibrators to rotation are presented for a number of standard interferometer configurations.

Online material: extended table, tar files

1. INTRODUCTION

A critical step in the practice of ground-based optical interferometry is the measurement of suitable calibrators (i.e., Mozurkewich et al. 2003). These allow compensation for various instrumental and atmospheric effects that reduce the measured fringe contrast. The ideal calibrator is bright (short of inducing nonlinearities in the detector) and has either an accurately known visibility or a diameter that can be reliably estimated to be small. In the latter case, stars that are bright and have small angular diameters are necessarily high-surface-brightness objects (i.e., early-type stars).

Early-type stars bring their own problems. In practice, the need to have calibrators relatively close to the science targets results in objects being chosen that have diameters that are larger than optimal. Unfortunately, as has been known almost since the inception of spectroscopy, stars earlier than F5 tend to rotate rapidly. This leads to oblate figures and significant gradients in surface temperature (von Zeipel 1924), resulting in visibilities that deviate from predictions by more than the error estimates, and even worse, visibilities that can change significantly with hour angle. Reflecting this fact, many lists

of calibrators (e.g., Bordé et al. 2002; Mérand et al. 2005) have excluded hot stars for the most part.

The actual rotation state of individual stars is rarely known, since the spectra give only the projected equatorial velocities $v \sin i$, usually interpreted only through line widths. Nevertheless, projected velocities can provide useful constraints on the range of the effects on the visibilities. In this paper, we use the theory developed by von Zeipel (1924) to estimate the visibilities over the range of parameters consistent with a star's observed magnitude, color, projected rotational velocity, and parallax, and its location in appropriate evolutionary grids.

In the next section, we describe the models and discuss their accuracy by comparing the diameters deduced from our calculated visibilities with measurements found in the literature. Furthermore, we have found that in many cases, the existence of a lower limit to the (polar) surface gravity imposed by the zero-age main sequence (ZAMS) provides an important constraint on the range of possible inclinations, and in § 3 we describe its impact on the simulations. In § 4, we discuss the results for some representative examples.

We have compiled lists of early-type stars that might be used as calibrators. Using typical parameters for some currently operating interferometers, we characterize for each object the range of visibilities that might be induced by rotation. In § 5, we describe the selection of these objects and the format of the catalogs.

A preliminary report of this research has recently appeared (Yoon et al. 2006), in which we focused on the more practical

---

[1] Department of Physics and Astronomy, Stony Brook University, Stony Brook, NY; jyoon@grad.physics.sunysb.edu, dpeterson@astro.sunysb.edu.

[2] Remote Sensing Division, Naval Research Laboratory, Washington, DC; tarmstr@nrl.navy.mil, jhc@sextans.lowell.edu, gilbreath@nrl.navy.mil, pauls@nrl.navy.mil.

[3] Interferometrics, Inc., Herndon, VA; hschmitt@nrl.navy.mil.

[4] PCPION, South Setauket, NY; rzagarello@mail.astro.sunysb.edu.

aspects of rotation and the calibration problem. Some details that we skip here can be found in that report.

2. THE EARLY-TYPE STARS AS CALIBRATORS

2.1. The Theory of Rotating Stars

The theory of rotating stars was studied by von Zeipel in 1924. He showed that stars in solid-body rotation will adopt the figure of a Roche spheroid to first order. He further showed that if radiative equilibrium holds, the emergent flux varies over the surface proportionally to effective gravity; that is, effective temperature is proportional to the fourth root of the local effective gravity. This theory has been tested not only in close binary systems, but also through interferometric observations of isolated stars (e.g., Domiciano de Souza et al. 2005; Peterson et al. 2006a, 2006b; van Belle et al. 2006).

2.2. The Visibility Calculations

The calculation of the visibilities was carried out as described in Peterson et al. (2006a). Briefly, given values for the Roche parameters (e.g., § 3.1), the position angle of the rotational axis, and the orientation of the projected interferometer baseline, we construct a grid of points across the projected disk of the star, with axes parallel and perpendicular to the projected baseline.

Following the developments in Collins (1963) and Hardorp & Strittmatter (1968), we calculate local surface values of effective temperature, effective gravity, and the direction of the normal at the grid points, and using the Kurucz (1993) models as parameterized by Van Hamme (1993), the specific intensity along the viewing angle. Intensities perpendicular to the baseline are summed, creating the "strip brightness distribution" (SBD). The Fourier transform of each pixel along the baseline, taken as a hat function, is calculated. The result is weighted according to the normalized SBD, multiplied by a phasor according to the "shift theorem" (Bracewell 1965), and summed to produce an approximate complex visibility $\tilde{V}$ (Born & Wolf 1999). The squared visibility is then simply $V^2 = \tilde{V}\tilde{V}^*$. We do not treat the related issue of the problems created for phase measurements due to rotation of the calibrators (Peterson et al. 2006a).

2.3. The Visibility Calibration

In what follows, we calculate the variations of the visibilities that are expected for a given star over the possible range of rotation parameters. The primary purpose of these calculations is to characterize the range of visibilities, but it is also of interest to know how reliable the calculated visibilities are themselves.

A good check is to compare the angular diameters we would predict in the absence of rotation with the measured diameters reported in the literature. To this end, we list in Table 1 the long-baseline angular diameters (θ_{meas}) for all stars listed in the Catalog of High Angular Resolution Measurements (Richichi

et al. 2005) in this color range, taking care to eliminate multiple references to the same measurements. Since our calculated diameters (θ_{calc}) implicitly include limb-darkening, in the few cases in which only uniform disk diameters are quoted, it is necessary to correct for limb-darkening effects. This was done with the simple device given by Hanbury Brown et al. (1974), using linear limb-darkening coefficients appropriate for the star's temperature and the bandpass of the observations from Van Hamme (1993).

The comparison between our photometric-based calculated diameters and the measurements is shown in Figure 1. Systematic differences are quite small. We have solved separately for possible additive ($\theta_{meas} = \theta_{calc} + a$) or multiplicative ($\theta_{meas} = b\,\theta_{calc}$) offsets. The solid line in Figure 1 shows the best least-squares fit for the additive case, $a = 0.084 \pm 0.026$ mas. The result for the multiplicative offset, $b = 1.019 \pm 0.007$, which for clarity we do not show, is comparably small. We conclude that our visibility calculations are systematically reliable for stars in this spectral region.

On the other hand, it is evident that the scatter is fairly large in Figure 1, and indeed we deduce reduced χ_ν^2's of 12.15 and 13.93 for the additive and multiplicative cases, respectively. This we attribute primarily to the effects of rotation, which are explicitly not modeled in the calculations or measurements. This explanation can easily accommodate β Cas and α Aql. The large residuals for α CMi (Procyon; at F5V, the coolest object in this list) are a puzzle and may originate in the effects of shallow convection, as discussed by Robinson et al. (2005) and Aufdenberg et al. (2005).

3. SIMULATIONS AND INTERPRETATION

In order to consistently estimate the visibilities and accurately estimate the variations induced by rotation, we cannot simply use angular diameters provided by the usual color-magnitude-diameter relations (i.e., Barnes et al. 1978, hereafter BEM78; Mozurkewich et al. 2003). Instead, we must calculate models that are consistent with each star's color and magnitude and with its other measured properties over the range of allowed inclinations and position angles. We describe those calculations next.

3.1. The Simulations

Roche models require several parameters: inclination angle i, mass M, angular diameter θ (or equivalently, the radius R through the parallax p), polar effective temperature $T_{eff, p}$, and the dimensionless angular velocity ω ($=\Omega/\Omega_B$, where Ω_B is the angular velocity at breakup). Starting with initial guesses of mass and temperature, we iterate until we match $v \sin i$ by varying the angular velocity parameter (ω) or inclination angle (i). Within this iteration, the program must also iterate for consistent values of $T_{eff, p}$ and θ_p to match the observed V magnitudes and $B - V$ colors. With values for ω, i, $T_{eff, p}$, θ_p, parallax, and an assumed mass, we can calculate the polar radius

TABLE 1
MEASURED VALUES AND CALCULATED VALUES OF ANGULAR DIAMETER

HR	Name	θ_{calc}	θ_{meas}	Bandpass	References
21	11 β Cas	1.89	2.12 $\pm$ 0.05	740 nm	1
82	27 ρ And	0.55	0.66 $\pm$ 0.08*	H, K	2
269	37 μ And	0.67	0.67 $\pm$ 0.11*	H, K	2
2421	24 γ Gem	1.40	1.39 $\pm$ 0.09	443 nm	3
2491	9 α CMa	6.12	6.04 $\pm$ 0.02	K	4
			5.89 $\pm$ 0.16	443 nm	3
			5.99 $\pm$ 0.11	800, 451 nm	5
2943	10 α CMi	5.03	5.45 $\pm$ 0.05	K	6
			5.45 $\pm$ 0.05	451, 550, 800 nm	5
			5.50 $\pm$ 0.17	443 nm	3
			6.44 $\pm$ 0.25	706 nm	7
			5.46 $\pm$ 0.08	740 nm	8
4090	30 LMi	0.54	0.59 $\pm$ 0.06*	H, K	2
4534	94 β Leo	1.34	1.31 $\pm$ 0.09*	443 nm	3
5447	28 σ Boo	0.69	0.78 $\pm$ 0.04*	H, K	9
6556	55 α Oph	1.54	1.63 $\pm$ 0.13	443 nm	3
6629	62 γ Oph	0.60	0.65 $\pm$ 0.06*	H, K	2
7001	3 α Lyr	3.20	3.23 $\pm$ 0.03	451, 500, 800 nm	5
			3.24 $\pm$ 0.07	438.5 nm	3
			3.28 $\pm$ 0.01	K	10
7469	13 θ Cyg	0.71	0.71 $\pm$ 0.06*	H, K	11
			0.85 $\pm$ 0.08*	H, K	12
7557	53 α Aql	3.05	3.46 $\pm$ 0.04	451, 550, 800 nm	5
			2.98 $\pm$ 0.14	460.8 nm	3
8162	5 α Cep	1.44	1.52 $\pm$ 0.07*	656 nm	13

REFERENCES.—(1) Nordgren et al. 1999; (2) Lane et al. 2001; (3) Hanbury Brown et al. 1974; (4) Kervella et al. 2003; (5) Mozurkewich et al. 2003; (6) Kervella et al. 2004; (7) Shao et al. 1988; (8) Nordgren et al. 2001; (9) Boden et al. 2000; (10) Ciardi et al. 2001; (11) Boden & Lane 2001; (12) Torres et al. 2002; (13) Vakili et al. 1998.

NOTE.—Asterisk (*) denotes measurements we have corrected to account for limb-darkening as described in the text.
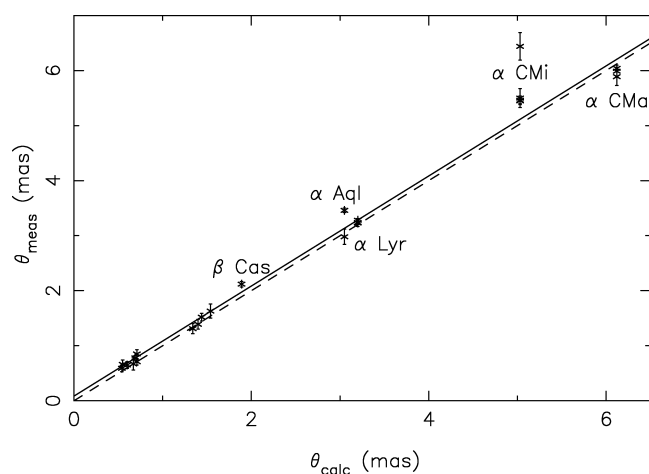

FIG. 1.—Comparison between measured and calculated angular diameters of early-type stars. The dashed line at 45° represents perfect agreement, while the solid line shows the least-squares fit of the measurements to the calculated values with an additive offset (of 0.084 $\pm$ 0.026 mas). The deviations of β Cas and α Aql are probably due to rotation.

and luminosity. Interpolation in the Claret grid (Claret 2004), assuming solar composition, yields a new mass estimate (e.g., Peterson et al. 2006a). The entire process typically converges to a fraction of a percent in mass in a few iterations.

Once the low inclination limit is established (at $\omega = 0.999$ or as limited by the ZAMS gravity; see below), we sample the visibilities over the allowed range of inclinations and position angles. To keep calculations as realistic as possible, in the catalogs and the examples discussed below, the visibilities are calculated assuming the object is on the meridian, and we account explicitly for its zenith distance for each specific observatory.

3.2. The ZAMS Constraint

In the process of conducting these simulations, we have found that the deduced polar gravity log g_p increases monotonically as the inclination angle decreases, with the projected velocity held fixed. Figure 2 shows two examples of this, for β Leo (HR 4534) and ζ Vir (HR 5107). Figure 2a illustrates the case of β Leo, whose polar gravity (*solid line*) always exceeds the polar gravity of the predicted ZAMS (*dotted line*). In such cases, we assume they are viewed equator-on only and are considered to be on the ZAMS within observational error
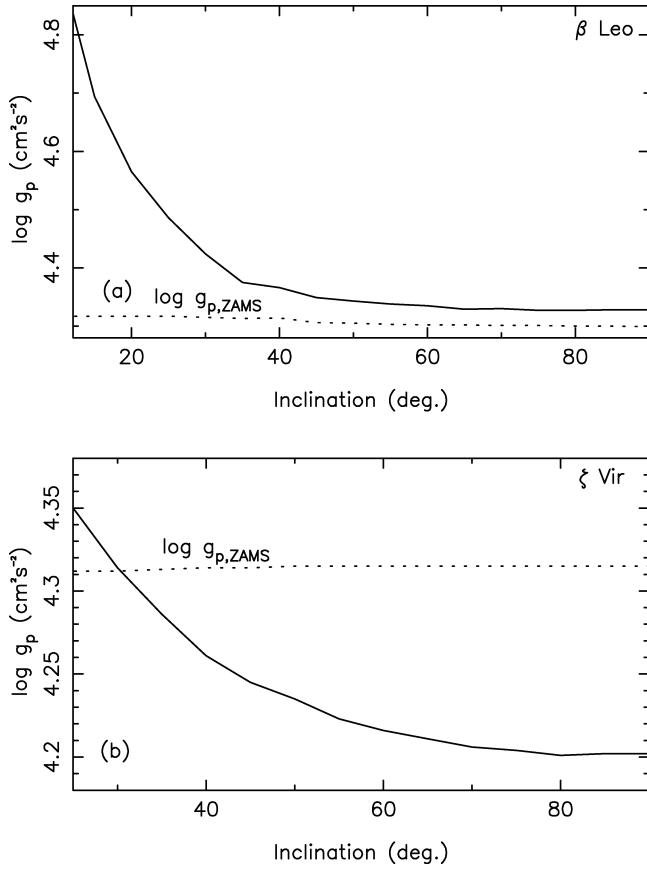
FIG. 2.—Relationships between polar gravity (the logarithm) and inclination of (*a*) β Leo and (*b*) ζ Vir (*solid lines*). The inclination covers the range from equator-on to breakup ($\omega = 0.999$). The dotted line shows the polar gravity at the ZAMS. β Leo has a larger polar gravity than if it were on the ZAMS with its predicted mass for all inclinations. In such cases, we assume it is viewed at $i = 90°$. The permitted range of inclinations for ζ Vir is terminated well before breakup ($\omega = 0.978$) by the ZAMS constraint.

and uncertainties in composition. ζ Vir, shown in Figure 2*b*, illustrates the case in which the potential range of the inclinations is terminated before reaching the inclination corresponding to breakup, here taken to be $\omega = 0.999$.

3.3. Statistical Calculations

Once the range of possible inclinations is established, V^2 is tabulated over a grid of 20 evenly spaced position angles and 20 inclinations. From this tabulation, we generate histograms describing the probability density function and calculate the maximum, minimum, average, and 68.3% (1 σ) confidence interval of V^2, found by splitting the out-of-range probability equally on the two sides (see Yoon et al. 2006 for details). The assumption here is that the rotational axis is randomly oriented in space over the range of allowed inclinations and position angles (e.g., Deutsch 1969).

4. RESULTS

We illustrate the range of results with four cases listed in Table 2. They include a slow rotator (HR 1673), an intermediate rotator (HR 8615), a moderately fast rotator (HR 3974), and a fast rotator (HR 7740). We have used appropriate instrument parameters for the 80 m baseline at the Navy Prototype Optical Interferometer (NPOI; Armstrong et al. 1998), operating at a wavelength of 500 nm. Note that by usual standards, these four objects would at first glance be good calibrator choices for the 80 m baseline at the NPOI, with angular diameters nominally in the range of 0.5–0.6 mas.

To put the calculations into context, we note that estimates of inferred angular diameters using surface brightness–angular diameter relations are typically uncertain by a few percent. Adopting the 3% uncertainty suggested by Mozurkewich et al. (2003), a star with a uniform disk angular diameter of $\theta = 0.55$ mas, measured with a 80 m baseline at 500 nm, has a visibility $V^2 = 0.63$, which is uncertain by about ± 0.02. The effects of rotation on the visibilities can be substantially larger than this.

Table 2 presents the results of the simulations for these four objects, giving V^2_{max}, V^2_{min}, $\bar{V}^2$, and $\pm \sigma$ values of the squared visibilities of each star. The histograms for the distribution of the V^2's derived from these calculations are shown in Figure 3. The bin size for the histograms is a tenth of the maximum-to-minimum range of squared visibility if the range is larger than 2% of $\bar{V}^2$; otherwise, it is fixed at 0.2% of the average if the range is less than 2% of $\bar{V}^2$.

TABLE 2
EXAMPLES OF EFFECTS OF ROTATION ON POTENTIAL CALIBRATORS (NPOI 80 m BASELINE AT $\lambda = 500$ nm)

HR	Name	Sp. Type	V	$B - V$	$v \sin i$ (km s⁻¹)	θ_{BEM78}[a] (mas)	p[b] (mas)	V^2_{max}	V^2_{min}	$\bar{V}^2$	$-\sigma$	$+\sigma$
1673	68 Eri	F2 V	5.12	0.44	10	0.606	39.99	0.6610	0.6298	0.6306	0.6304	0.6306
3974	21 LMi	A7 V	4.48	0.18	148	0.546	35.78	0.6881	0.6778	0.6829	0.6783	0.6874
7740	33 Cyg	A3 IV–Vn	4.30	0.11	268	0.533	21.41	0.7555	0.6054	0.6530	0.6272	0.6787
8615	31 Cep	F3 III–IV	5.08	0.39	85	0.571	17.70	0.7102	0.6486	0.6576	0.6505	0.6632

NOTE.—Data represent examples of the effects of rotation on potential calibrators as measured by the maximum, minimum, weighted average, and $\pm \sigma$ values of V^2 using the NPOI (80 m baseline at $\lambda = 500$ nm).

[a] Angular diameter θ_{BEM78} from the Barnes et al. (1978) relation, for guidance only.
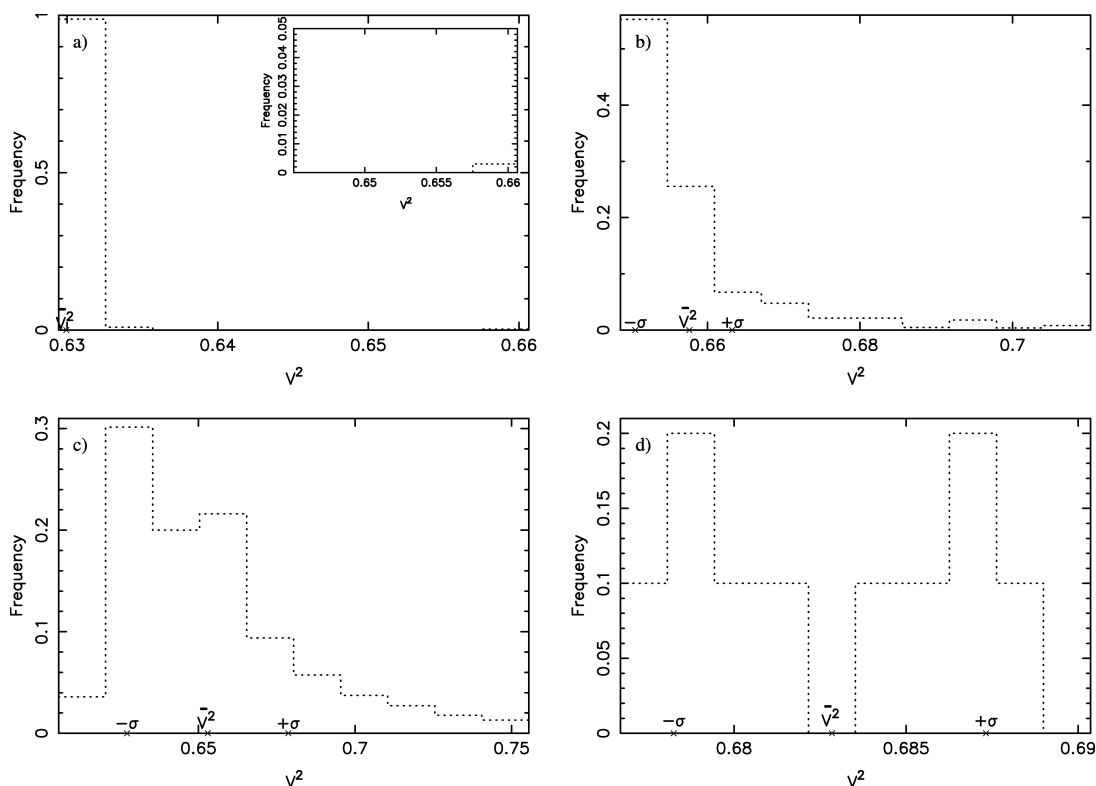
[b] Parallax p from *Hipparcos* (ESA 1997).

FIG. 3.—Histograms of squared visibilities. (*a*) HR 1673 (68 Eri) is a slow rotator with $v \sin i = 10$ km s^{-1}. In spite of its slow rotation and narrow range of $\pm \sigma$, the histogram displays an extended tail, albeit of low probability, as shown in the inset. These extreme visibilities result from the fact that the star could be seen nearly pole-on. (*b*) Histogram for HR 8615 (31 Cep), an intermediate-velocity rotator with $v \sin i = 85$ km s^{-1}. This star can be a calibrator, but the full range of squared visibilities should be properly considered, because of the extended tail of possible V^2 values, and particularly the asymmetric distribution. (*c*) HR 7740 (33 Cyg) is a fast rotator, with $v \sin i = 268$ km s^{-1}. As expected, the rotation significantly affects the visibilities. (*d*) Moderately rotating star, HR 3974 (21 LMi), with $v \sin i = 148$ km s^{-1}, which is on or very near the ZAMS and is therefore assumed seen equator-on. This can be a good calibrator, because of the small predicted range in V^2, owing to the constrained range of inclination.

The usual assumption that slow projected rotation assures no significant effects from rotation is not so reliable. The slow rotator HR 1673 (Fig. 3*a*) shows an extended, low-probability tail in squared visibility. Even though the 1 σ confidence interval for this object is very small, there is a finite chance of introducing a 4% error. In the simulations for this star, the inclination was cut off at an inclination of $i = 2.45°$, with smaller inclinations pushing the models below the ZAMS. Even with critical rotation excluded, the high inclination that is accessible can generate significant uncertainties in the visibilities.

Figure 3*b* shows the corresponding histogram for HR 8615, which would normally be considered a slow rotator for these stars, with a projected rotational velocity of 85 km s^{-1}. The histograms show a rather different story, with a wing on the distribution to higher squared visibilities amounting to 10% of the mean value. Thus, although this object appears to be as reasonable a candidate for a calibrator as HR 1673, it should be used only if nothing else is available.

For the moderately fast rotator HR 7740 ($v \sin i = 268$ km s^{-1}; Fig. 3*c*), we see the expected effects on the predicted squared visibilities. Significant flattening is predicted at all inclinations, so the visibility measurements vary significantly over the possible combinations of inclination and position angle. In spite of a small predicted angular diameter, 0.533 mas, the range in visibilities must be considered if calibrating with this star.

Finally, Figure 3*d* shows how the ZAMS constraint affects the visibility range of a star with moderately fast projected rotation: HR 8615, with $v \sin i = 148$ km s^{-1}. This star appears to lie near but slightly below the ZAMS (which we interpret to mean that it is on the ZAMS to observational limits), which greatly limits the predicted range of visibilities. We predict HR 8615 would be a good calibrator, in spite of its significant projected velocity. The double-horned shape of the resulting histogram is characteristic of stars that display significant rotation and are near the ZAMS.

From these examples, it is clear that the probability density functions for the squared visibilities are distinctly non-Gaussian, and there is a significant question of how best to characterize their shapes. For the catalogs, we have decided to limit

TABLE 3
NPOI 80 m Baseline (λ = 500 nm) Catalog

HR (1)	Name (2)	α (J2000.0) (3)	δ (J2000.0) (4)	Sp. Type (5)	V (6)	B − V (7)	v sin i (8)	p (9)	$V^2_{\max}$ (10)	$V^2_{\min}$ (11)	$\bar{V}^2$ (12)	−σ (13)	+σ (14)	Q (15)	E (16)
82 …….	27ρ And	00 21 07.3	+37 58 07	F5 III	5.18	0.42	41	20.42	0.7019	0.6494	0.6528	0.6502	0.6540	A	−
269 ……	37μ And	00 56 45.2	+38 29 58	A5 V	3.87	0.13	72	23.93	0.5870	0.5221	0.5297	0.5242	0.5330	A	−
343 ……	33θ Cas	01 11 06.2	+55 08 59	A7 V	4.33	0.17	102	23.73	0.6910	0.6338	0.6426	0.6358	0.6469	A	−
417 ……	48ω And	01 27 39.4	+45 24 24	F5 IV	4.83	0.42	69	35.33	0.6183	0.5496	0.5563	0.5510	0.5598	A	−
531 ……	53χ Cet	01 49 35.1	−10 41 11	F3 III	4.67	0.33	61	42.35	0.6152	0.6080	0.6103	0.6089	0.6115	A	0

Note.—Table 3 is published in its entirety in the electronic edition of the *PASP*. A portion is shown here for guidance regarding its form and content. Units of right ascension are hours, minutes, and seconds, and units of declination are degrees, arcminutes, and arcseconds. Col. (15): A, B, and C characterize the 1 σ width of the visibility distribution (see text); col. (16): the characters +, 0, and − indicate how extended the tails in the visibility distributions are (see text).

the quantitative description to simply listing the mean, the 1 σ confidence interval, and the extreme values of the squared visibilities. Since these are a rather minimal set of parameters, given the obviously complex shapes involved, we have decided to include graphs of the histograms for these objects along with the archived tables.

We have assumed solar composition throughout these calculations. To see how sensitive these results are to composition, we have run the simulations in a few representative cases with $Z = 0.03$ (using for this purpose the Padova grid [Girardi et al. 2000], where $Z = 0.019$ is solar composition). With the higher metallicity, the deduced masses are larger, as expected. However, the deduced diameters decrease only slightly, and in turn the visibilities are minimally affected. In the range of diameters encountered here, the mean squared visibilities typically increase by 0.3%, with an occasional case reaching 1%. We conclude that the predictions here are not sensitive to composition so long as it is not too far from solar.

5. CATALOGS

The extent to which rotation introduces errors in the calibration process depends on the wavelengths and baselines used. We consider three instruments here: the NPOI, working at 500 nm, the array at the Center for High Angular Resolution Astronomy (CHARA; ten Brummelaar et al. 2005) operating at the *K* band, and the Very Large Telescope Interferometer (VLTI; Glindemann et al. 2003), also at the *K* band.

For the northern instruments, our input list of potential calibrators satisfies the following criteria: (1) luminosity class III, IV, and V stars in the color range $B − V \leq 0.45$, as listed in the Bright Star Catalogue (BSC; Hoffleit & Warren 1991),[5] (2) declinations above −15°, (3) angular size θ_{BEM78}, estimated using the surface brightness–angular diameter relation of BEM78 between 0.5 and 1.0 mas, and (4) distance closer than 100 pc (the last eliminates significant reddening). We then pruned the list of any stars with companions with separations $\rho \leq 1''$ and magnitude differences $\Delta m < 5.0$, and of all confirmed spectroscopic binaries.

A separate list with the same characteristics but with a dec-

lination range of −90° $\leq \delta \leq$ +15° was used for the VLTI catalog.

The spectroscopic binary (SB) issue is complicated for the B, A, and F stars and requires further comment. The A stars in particular are subject to a variety of nonradial pulsation modes (δ Scuti, δ Delphini, etc.) and inhomogeneous surface composition that, coupled with rotation, lead to time-variable structure in the line profiles. These have on numerous occasions led to reports of multiple spectra, radial velocity variability, and even preliminary SB1 orbits that were later questioned or retracted (e.g., Abt & Levy 1974). Unfortunately, once listed, the "SB" classification has rarely been expunged from the BSC. The majority of the A stars in our original candidate list were characterized as SB. We have therefore removed objects reported as SB (of any flavor) only if a critical evaluation of the orbit has led to the object's inclusion in the Ninth Spectroscopic Binary Catalogue (Pourbaix et al. 2005).[6] Failing this, we have retained the object in our catalog. As a result, we expect that there will be binaries lingering in these lists, and we repeat the caution to always observe a check star as well as a primary calibrator. *K*-band observations will be particularly susceptible to these problems.

We have calculated catalogs for five specific configurations. Our main interest is in establishing reliable calibrators for the NPOI, and three of the configurations are for the 64, 80, and 100 m baselines (AE–W7, E6–W7, and E7–W7; Armstrong et al. 1998). In addition, to illustrate the wavelength dependence of the results, a catalog has been compiled for the 331 m CHARA arm (S1–E1; ten Brummelaar et al. 2005). A wavelength of 2.22 μm was adopted, typical of the *K* band but offset enough from band center to avoid Brγ, which is a very strong feature in these objects. Finally, to extend this to the Southern Hemisphere, we have compiled a fifth catalog using the parameters for the 140 m VLTI arm (B3–MO; Glindemann et al. 2003), also at 2.22 μm.

While these five catalogs are directly usable for the instruments and configurations indicated, they also provide some general guidance as to the reliability of individual objects as calibrators. However, for instruments and configurations far from those con-

sidered, we would be glad to make additional runs, given the instrumental details (contact the first author, J. Y.).

The catalogs consist of a text file of stars and their visibility information, as shown in Table 2, and a separate archive of postscript files containing histograms: CHARA 331 m, NPOI 64 m, NPOI 80 m, NPOI 100 m, and VLTI 140 m, available as electronic files in the electronic edition of the *PASP*. Table 3 shows the first few entries of the NPOI 80 m baseline catalog, which includes the HR number, name, α and δ (J2000.0), spectral type, V magnitude, $B - V$ color, projected rotational velocity ($v \sin i$, primarily from the BSC), parallax p, V_{max}^2, V_{min}^2, $\bar{V}^2$, $-\sigma$, and $+\sigma$ (in cols. [1]–[14], respectively). The last two columns, labeled Q and E, give a rough indication of the quality of each object as a calibrator. In the column labeled Q, the

calibrator is classified as A if $\Delta\sigma/\bar{V}^2 \leq 0.02$, B if $0.02 < \Delta\sigma/\bar{V}^2 \leq 0.04$, and C otherwise, where $\Delta\sigma = (+\sigma) - (-\sigma)$. The last column, E, classifies a calibrator plus, zero, or minus if, respectively, $(V_{max}^2 - V_{min}^2)/\Delta\sigma \leq 2$, is between 2 and 4, or is greater than 4. The E classification is meant to warn of cases in which one might be "exposed" to large error in V^2, even when $\Delta\sigma$ is small and the probability of such exposure is small. The histograms have a format similar to the figures shown in this paper.

REFERENCES

Abt, H. A., & Levy, S., G. 1974, ApJ, 188, 291
Armstrong, J. T., et al. 1998, ApJ, 496, 550
Aufdenberg, J. P., Ludwig, H.-G., & Kervella, P. 2005, ApJ, 633, 424
Barnes, T. G., Evans, D. S., & Moffett, T. J. 1978, MNRAS, 184, 285 (BEM78)
Boden, A. F., Creech-Eakman, M. J., & Queloz, D. 2000, ApJ, 536, 880
Boden, A. F., & Lane, B. F. 2001, ApJ, 547, 1071
Bordé, P., et al. 2002, A&A, 393, 183
Born, M., & Wolf, E. 1999, Principles of Optics (7th ed.; Cambridge: Cambridge Univ. Press)
Bracewell, R. 1965, The Fourier Transform and Its Applications (New York: McGraw-Hill)
Ciardi, D. R., et al. 2001, ApJ, 559, 1147
Claret, A. 2004, A&A, 424, 919
Collins, G. W., II 1963, ApJ, 183, 1134 (erratum, 139, 1401 [1964])
Deutsch, A. J. 1969, in Stellar Rotation, ed. A. Slettebak (New York: Gordon and Breach), 207
Domiciano de Souza, A., et al. 2005, A&A, 442, 567
ESA. 1997, The Hipparcos and Tycho Catalogues (ESA SP-1200; Noordwijk: ESA)
Girardi, L., et al. 2000, A&AS, 141, 371
Glindemann, A., et al. 2003, Proc. SPIE, 4838, 89
Hanbury Brown, R., Davis, J., & Allen, L. R. 1974, MNRAS, 167, 121
Hanbury Brown, R., Davis, J., Lake, R. J. W., & Thompson, R. J. 1974, MNRAS, 167, 475

Hardorp, J., & Strittmatter, P. A. 1968, ApJ, 151, 1057
Hoffleit, D., & Warren, W. H., Jr. 1991, Bright Star Catalogue (5th rev. ed.; New Haven: Yale Univ. Obs.)
Kervella, P., et al. 2003, A&A, 408, 681
———. 2004, A&A, 413, 251
Kurucz, R. L. 1993, Kurucz CD-ROM 13, ATLAS9 Stellar Atmosphere Programs and 2 km/s Grid (Cambridge: SAO)
Lane, B. F., Boden, A. F., & Kulkarni, S. R. 2001, ApJ, 551, L81
Mérand, A., Bordé, P., & Coudé du Foresto, V. 2005, A&A, 433, 1155
Mozurkewich, D., et al. 2003, AJ, 126, 2502
Nordgren, T. E., et al. 1999, AJ, 118, 3032
Nordgren, T. E., Sudol, J. J., & Mozurkewich, D. 2001, AJ, 122, 2707
Peterson, D. M., et al. 2006a, ApJ, 636, 1087
Peterson, D. M., et al. 2006b, Nature, 440, 896
Richichi, A., Percheron, I., & Khristoforova, M. 2005, A&A, 431, 773
Pourbaix, D., et al. 2005, A&A, 424, 727
Robinson, F. J., et al. 2005, MNRAS, 362, 1031
Shao, M., et al. 1988, ApJ, 327, 905
ten Brummelaar, T. A., et al. 2005, ApJ, 628, 453
Torres, G., et al. 2002, AJ, 124, 1716
Vakili, F., et al. 1998, A&A, 335, 261
van Belle, G. T., et al. 2006, ApJ, 637, 494
Van Hamme, W. 1993, AJ, 106, 2096
von Zeipel, H. 1924, MNRAS, 84, 684
Yoon, J., et al. 2006, Proc. SPIE, 6268, 626848